Electronic Supplementary Information

Mn valence calculation of the precursor in the S_0 sample

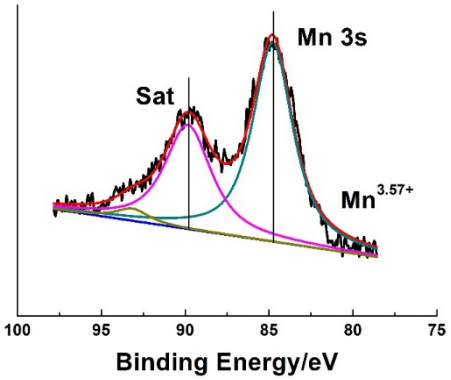

Fig. S1 the XPS Mn 3s region of the precursor in the S_0 sample.

Splitting of transition metal 3s XPS spectrum occurred due to exchange coupling between the 3s hole and 3d electrons. The difference in binding energy between the Mn 3s peak and its' satellite peak (ΔE) was used to approximate the average Mn oxidation state (AOS) by the equation, AOS = 8.956−1.126 ΔE. [27] Thus the calculated average Mn oxidation state of the precursor was +3.57.

Comparison experiment without $(NH_4)_2S_2O_8$

$KMnO_4$ and $MnSO_4$ were dissolved at a molar ratio of 0.3:0.7, 0.35:0.65, 0.4:0.6 and 0.45:0.55 in 10 mL of deionized water in a Teflon liner to obtain a mixed solution. Afterward, 20 mL LiOH solution (3 mol/L) was trickled into the mixture, which was stirred for 30 min to yield a precursor precipitate. The Teflon liner was transferred to an autoclave and maintained at 200 °C for 24 h. The as-prepared powders were filtered, washed, and dried at 80 °C for 24 h. The obtained samples were referred to as C_1, C_2, C_3, and C_4, respectively, in which the Mn valence of the precursor were 3.5, 3.75, 4.0 and 4.25.

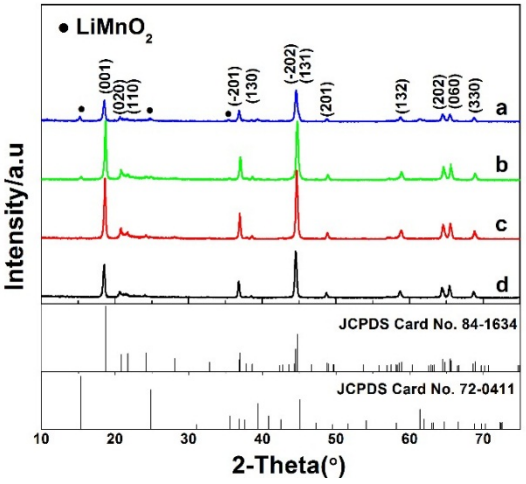

Fig. S2 the XRD patterns of the samples, (a) for C_1, (b) for C_2, (c) for C_3 and (d) for C_4.

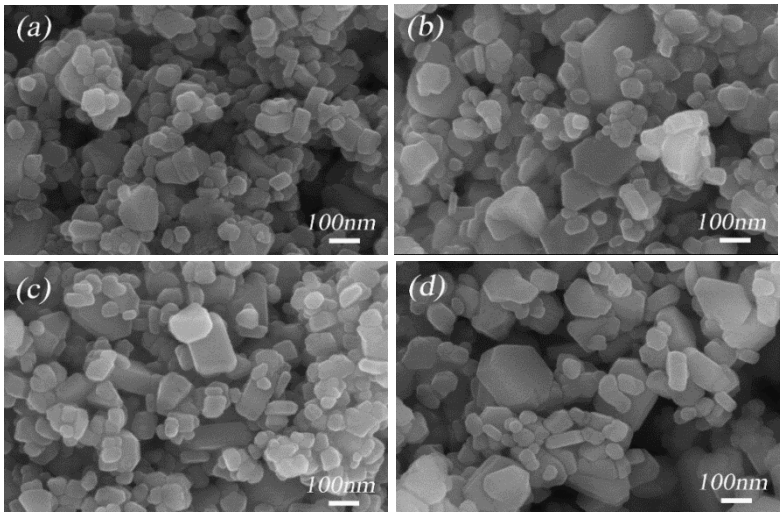

Fig. S3 SEM images of the samples, (a) for C_1, (b) for C_2, (c) for C_3 and (d) for C_4.

The phase compositions of the products without $(NH_4)_2S_2O_8$ were analyzed by XRD (Fig. S2). While the Mn valence varied from +3.5 to +4, a main phase of Li_2MnO_3 with small amounts of O–$LiMnO_2$ was observed. Furthermore the increasing Mn valence led to less $LiMnO_2$. The XRD patterns of the samples showed a single Li_2MnO_3 phase when the Mn valence exceeded +4. These results indicated that the precursor changed without $(NH_4)_2S_2O_8$, as the poor oxidizing ability of $KMnO_4$ in alkaline solution. Thus, the addition of $(NH_4)_2S_2O_8$ was significant for oxidizing the precursor.

The morphologies of the products of C_1-C_4 were observed by SEM in Fig. S3. All the samples showed bulk shape with 50nm particles and larger particles with 200-300nm size. Furthermore the grain sizes did not show obvious change while the average Mn valence of the precursor varied from 3.5 to 4.25. It referred to the change of the precursor without $(NH_4)_2S_2O_8$. $MnSO_4$ could not be oxidized completely to δ-MnO_2 by $KMnO_4$. The synthesis process was more complex and hardly controlled.

The second charge/discharge curves of the S_6-S_{20} samples

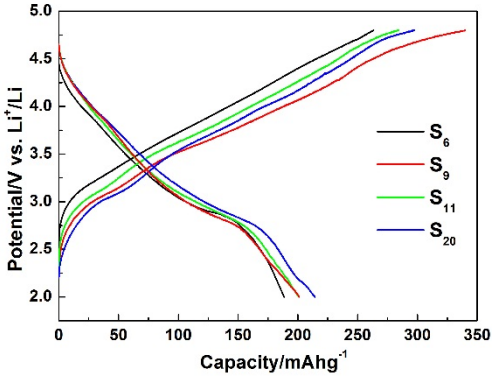

Fig. S4 the second charge and discharge curves of the S_6-S_{20} samples.

The cycle performance of S_6-S_{20} samples

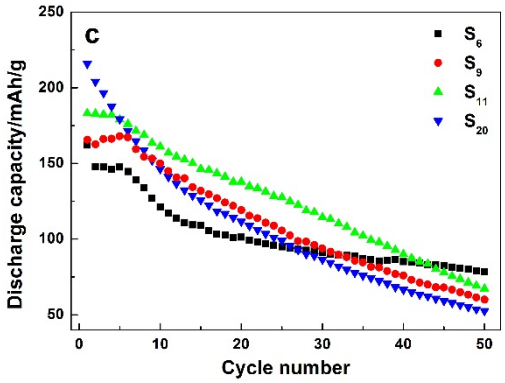

Fig. S5 the cycle performance at 100mAh/g of the S_6, S_9, S_{11} and S_{20} samples.

Fig. S5 demonstrated the cycle performance of S_6, S_9, S_{11}, and S_{20} at a rate of 100 mA/g (1st-50th). The first discharge capacities were 162, 166, 183, and 210 mAh/g, while the capacity retentions were 48.5%, 36.1%, 36.7% and 25% after 50 cycles for S_6, S_9, S_{11}, and S_{20}, respectively. S_6 capacity demonstrated a fast fade during the 5th -15th cycles, followed by a slow and linear fade after the 16th cycle. The capacities of S_9 and S_{11} showed linear fade after the 5th cycle. On the contrary, nearly logarithmic decrease of the discharge capacity was observed in S_{20} samples. The poor cycling stability in S_9-S_{20} samples might arise from the interfacial reactions and electrolyte erosion. In summary, decreasing grain sizes led to larger initial discharge capacities and lower capacity retentions after 50 cycles.

CV curves of S_6-S_{20} samples

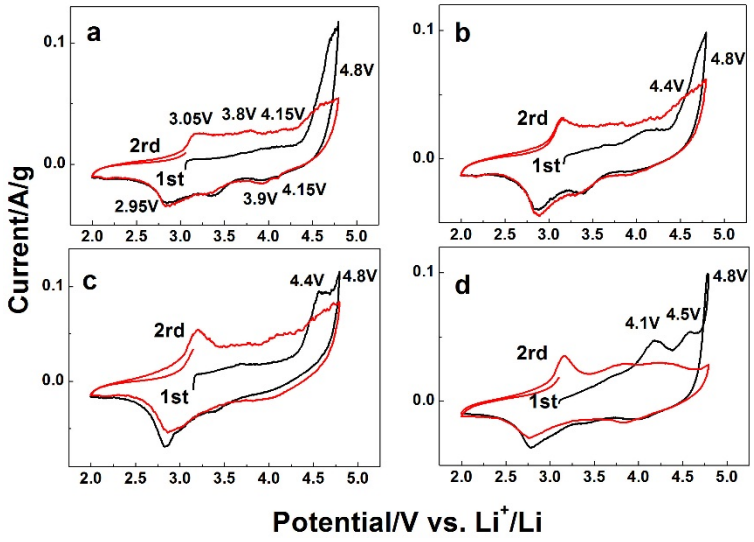

Fig. S6 Cyclic voltammograms (0.1 mV/s, 2-4.8V) of the first and second cycle, (a) for S_6, (b) for S_9, (c) for S_{11} and (d) for S_{20}.

CV measurements were carried out for S_6-S_{20} samples. As plotted in Figure S6, S_6, S_9, S_{11} and S_{20} showed different oxidation peaks in the initial cycle. In S_6 and S_9 samples, Li_2O-extraction peak overlapped with the 4.8V peak which arose from the interfacial reaction. A distinct oxidation peak appeared at ~4.4 V in S_{11} samples. By contrast, S_{20} demonstrated two peaks at 4.1 and 4.5 V. These results showed that Li_2O-extraction peaks shifted to lower voltages with decreasing sample size. The oxidation peak positions mainly consistent with the *dQ/dV* curves in the manuscript.

The curves of all samples were similar to each other in the second charge/discharge. As presented in Fig. S6, a distinct oxidation peak appeared at ~3.05V, whereas a reduction peak was observed at ~2.95V. Two weak oxidation peaks at ~3.8V and 4.15V implied the existence of spinel phase with corresponding reduction peaks at ~3.9V and 4.15V. CV curves demonstrated a similar conclusion with the *dQ/dV* curves in the manuscript. The minor difference with *dQ/dV* curves arose from different charging and discharging method.